SSRG International Journal of Electrical and Electronics Engineering
ISSN: 2348-8379/ https://doi.org/10.14445/23488379/IJEEE-V11I7P126

Volume 11 Issue 7, 291-301, July 2024

Original Article

Performance Enhancement of Hybrid-Type Full-Bridge DC/DC Converter with Fuzzy MPPT for Efficient Photovoltaic Power Extraction

P. Kamalakar[1], B. Suresh Kumar[2], J. Upendar[3]

[1,3]*Electrical and Electronics Engineering Department, University College of Engineering, Osmania University, Telangana, India.*
[2]*Electrical and Electronics Engineering Department, CBIT, Telangana, India.*

[1]*Corresponding Author : kamalakarpothulapally@gmail.com*

Received: 12 May 2024 Revised: 15 June 2024 Accepted: 12 July 2024 Published: 26 July 2024

Abstract - *Renewable power utilization has become an essential requirement for the power grid system, replacing conventional fossil fuel generation. Power extraction from renewable sources is a complex task as the power generation is variable due to unpredictable natural sources. In this paper, an HTFB DC/DC converter is connected to a PV array for extracting maximum power. The HTFB is operated by a high-frequency pulse for the power electronic switches on the primary side of the converter. The duty ratio of these pulses is controlled by the MPPT technique, which takes references from PV voltage and current signals. A traditional INC MPPT is used for maximum power extraction from the PV array. This MPPT technique is updated to FLC MPPT for better stability and improved power extraction from the PV array. For testing and comparing these techniques, a grid connected inverter with an EV charging station is adopted. The inverter injects the extracted power by the HTFB into the grid and also sharing to the EV charging station. All the comparative results are generated using the Simulink environment of MATLAB software.*

Keywords - *HTFB (Hybrid type Full bridge), PV (Photo Voltaic), MPPT (Maximum Power Point Tracking), INC (Incremental Conductance), FLC (Fuzzy Logic Controller), EV (Electric Vehicle), Simulink, MATLAB (Matrix Laboratory).*

1. Introduction

With rising concerns about very high global temperatures, it is crucial time to choose renewable power generation for the load demand. For large grid systems high rated renewable sources with multiple modules are accumulated for load compensation. For miniature grids and micro grids single renewable source is connected in parallel to the conventional source for sharing power to the loads [1]. The micro grids have ratings in the range of kW, which needs efficient converters and controllers for maximum power delivery.

In conventional methods the renewable sources are connected to the grid through basic converters like boost converter, buck-boost converters and inverters. These conventional converters have very low efficiency and high ripple or harmonic content [2]. Buck-boost converters, due to their switching nature, can produce significant Electromagnetic Interference (EMI), which can affect nearby electronic devices. Therefore, careful design is necessary to mitigate this interference. In addition, buck-boost converters may have a higher output voltage ripple compared to buck or boost converters alone, potentially causing issues in applications that require a very stable voltage output. The efficiency of buck-boost converters can significantly decrease at the extremes of their input voltage and load ranges. Typically, efficiency is highest when the input voltage is close to the output voltage and the load is moderate.

To achieve high efficiency and power density, thermal management is crucial for buck-boost converters. This may involve the use of heat sinks or fans, which can increase the overall size and complexity of the system. Furthermore, buck-boost converters may have limitations on the amount of current they can handle, especially in applications requiring high output currents.

This leads to reduced renewable power injection into the grid, making it a failed system. Traditional controllers like voltage feedback current-oriented controllers also have high disturbances, creating oscillations in the system [3]. These traditional converters and controllers need to be replaced by advanced techniques for maximum power extraction and efficient sharing to the grid. The conventional boost converter is replaced with a Hybrid Type Full Bridge (HTFB) DC/DC

converter with high gain and efficiency [4]. All the drawbacks of the older converter are overcome by this HTFB converter, creating a more stabilized and efficient system. At the output of the HTFB, the circuit topology is a simple three phase inverter connected to the grid through an LC filter and step-up transformer [5]. As a local load an EV charging station is also integrated into the system for charging the EV battery pack by the solar renewable source. The below outline Figure 1 represents the structure of the proposed grid system with all the modules integrated into the grid.

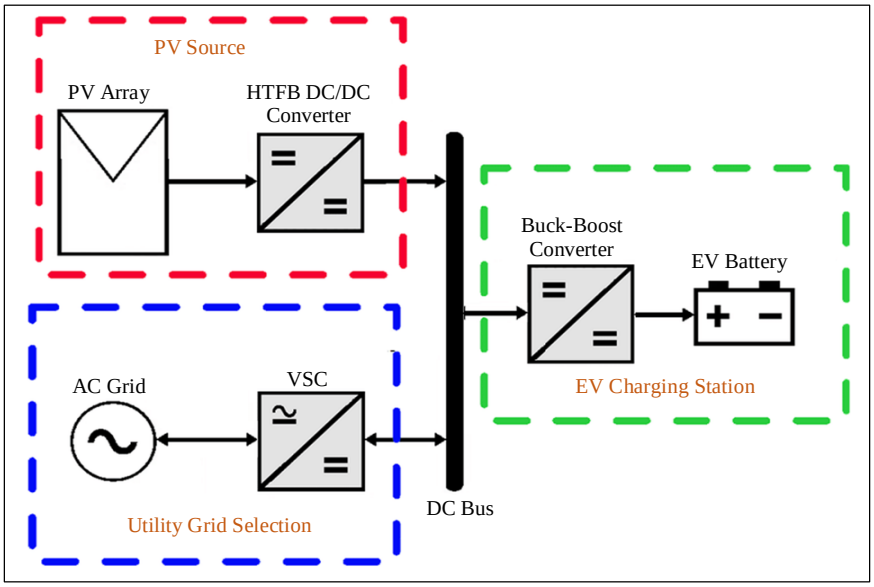

Fig. 1 Outline schematic of the proposed renewable grid system

As observed, the 'PV source' and the 'EV charging station' are unidirectional, and the 'Utility grid section' is bidirectional. The PV source needs converters which only extract power from PV panels and share it with the system. The EV charging station needs only a converter to charge the EV battery.

Whereas the Utility grid has to share power with the EV charging station or get power from a PV source during deficit and excess renewable power conditions, respectively, it is integrated with VSC (Voltage Source Converter) [6]. The VSC is an AC/DC bidirectional converter which operates are inverter or rectifier as per the EV charging station power demand and generated PV source power. The EV charging station has a simple Buck-Boost converter, which controls the charging current with the current controller.

In the PV source, the HTFB is a DC/DC converter controlled by the INC MPPT technique for maximum power extraction. Due to the limitations of INC MPPT, like a slower response to the changes and bad duty ratio estimation, the maximum power extraction and stability are not achieved. Therefore, the INC MPPT is replaced with FLC MPPT with the same signal feedback from the PV array, generating an optimal duty ratio with a faster response rate [7]. This paper is structured as follows:

- Introduction to the renewable grid system and its components in Section 1
- Configuration and design of the HTFB DC/DC converter connected to the PV source in Section 2
- Design and implementation of the FLC MPPT for the control of the HTFB converter in Section 3.
- Simulation analysis and comparison results with INC and FLC MPPT modules in PV source in Section 4.
- Conclusion validating the better MPPT module for PV source with maximum power extraction and stability in Section 5.

2. HTFB DC/DC Converter

The HTFB DC/DC converter is an advanced converter for high-rating DC/DC converting applications with very low ripple content. This converter can be adapted to systems with high current requirements (in the range of 50-100A) at high voltages (in the range of 300 – 500V). The rating of the system with a power transfer requirement of 50kW leads to several power quality issues like reduced efficiency, high ripple and oscillations in the output voltage [8].

This HTFB DC/DC converter is included with High Frequency Transformer (HFTF), which transfers this high rating power to the load. The HFTF can increase or decrease the voltage levels on the load side. Along with this capability of voltage magnitude variation, it protects the circuits from external faults as both the networks are mechanically coupled and electrically isolated by the HFTF. The circuit topology of the HTFB DC/DC converter is presented in Figure 2 in detail.

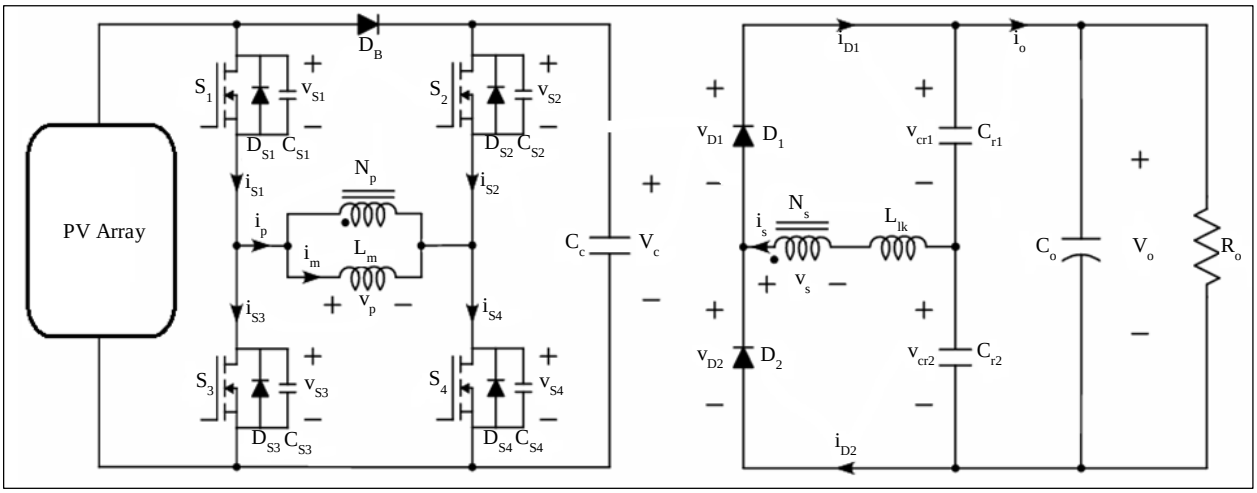

Fig. 2 HTFB DC/DC converter circuit topology

As per Figure 2, the PV array is connected to a full bridge inverter with four MOSFETs (Metal Oxide Field Effect Transistors) S1-S4. These MOSFETs are operated at very high frequencies in the range of 100kHz as per the requirement. The power from the PV array is extracted by the full bridge and converted to high frequency AC by the switching pulses fed to MOSFETs. The pulses to the MOSFETs are generated with a half cycle phase shift modulation technique discussed in the next section.

The MOSFET switches full bridge is connected to the primary side of the HFTF, which has a specific primary turns ratio (N_p) and transfers power to the secondary side with the same turns ratio (N_s) or different as per the requirement [9]. For increased voltage magnitude, the $N_s > N_p$ and for lower voltage, $N_s < N_p$. On the secondary side the winding is connected to a diode bridge with two resonating capacitors (C_{r1} and C_{r2}) replacing the diodes of one branch for DC voltage stability.

The output of the diode bridge with capacitors is connected to the load with a parallel output capacitor (Co) for DC voltage ripple reduction. The output terminals of the diode bridge are either connected to a local load, EV charging station or grid connected inverter. As the name suggests, the HTFB converter can operate in two modes: active clamping mode and resonant mode.

The active clamping mode is adopted for variable voltage conditions by varying the duty ratio of switches, keeping the phase shift exactly to half. In the other mode for resonant operation of the full bridge, the duty ratio is kept constant, but the phase of the pulses is varied [10]. As per the application with PV source input for maximum power extraction, the HTFB is operated in active clamping mode with a variable duty ratio. Figure 3 represents the switching signals and current waveforms of passive and active elements of the HTFB converter. The operating conditions of the HTFB as per pulse input to the MOSFET and the current conduction paths are explained in detail below.

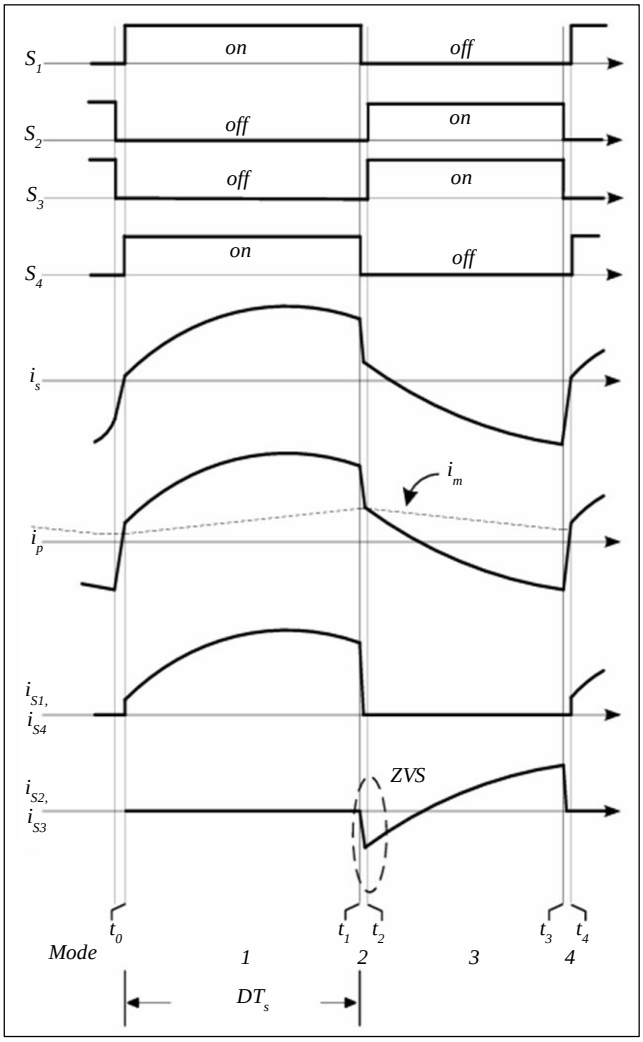

Fig. 3 Switching states and current of passive and active elements

In the active clamping mode, the switch pairs (S1 S4) and (S2 S3) are operated in a complimentary manner, creating an AC waveform [11].

State 1: In this state, the switches S1 and S4 are turned ON, creating a positive current conduction path in the primary winding. PV voltage (V_{pv}) is applied to mutual inductance (L_m) of the HFTF, which increases the magnetizing current linearly given as:

$$i_m(t) = i_m(t_0) + \frac{V_{pv}}{L_m}(t - t_0) \quad (1)$$

Here, 't_0' is the initial time of the S1 and S4 pulse and 't' is the present time. The current conduction path for state 1 can be observed in Figure 4.

On the secondary side, the diode D1 is forward biased, and the secondary side resonating current (i_s) is created between C_{r1}, C_{r2} and L_{lk} (Leakage inductance).

$$i_s(t) = i_s(t_1)\cos w_r(t - t_1) - \frac{nV_c - V_{cr2}(t_1)}{Z_r}\sin w_r(t - t_1) \quad (2)$$

Here 'n' is the turns ratio of the HFTF, w_r is the resonating angular frequency, Z_r is the impedance of the converter. The C_o is charged with the i_s, and the load receives voltage-elevated power [12].

State 2: In this mode, all the switches are turned OFF for a small instant of time, creating dead time for freewheeling. The current conduction path for state 2 is presented in Figure 5.

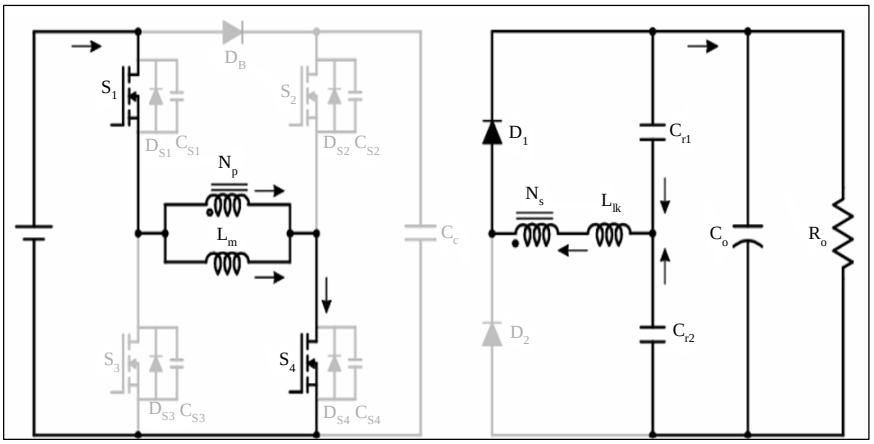

Fig. 4 State 1 operating condition

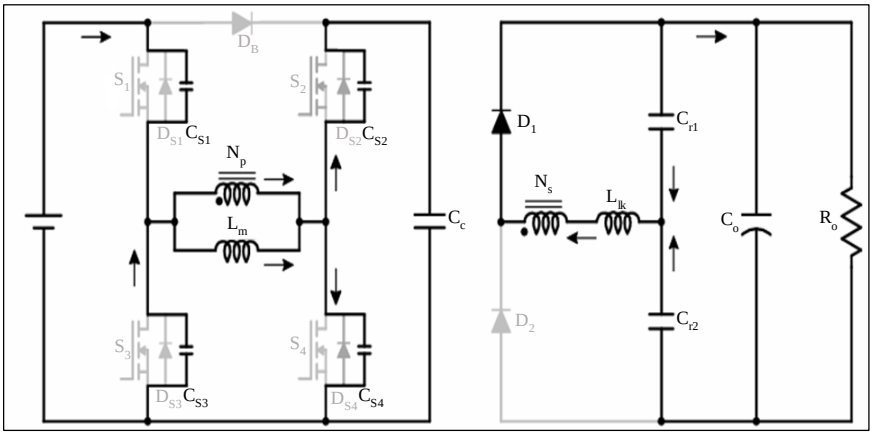

Fig. 5 State 2 operating condition

In this state, the capacitors C_{s1} and C_{s4} are charged with input primary current i_p, and C_{s2} and C_{s3} are discharged.

State 3: In this state, the switches S2 and S3 are turned ON creating negative voltage on the primary winding with reverse primary current conduction [12]. The current conduction path for state 3 can be observed in Figure 6.

In this state 3, the charged capacitor Cc creates a negative direction current path in the primary winding through S2 and S3. The negative voltage is transferred to the secondary side, and the diode D2 is now in forward bias condition. As the switch body capacitances (Cs1 – Cs4) are charged in state 2, the switches S2 and S3 are turned ON with Zero Voltage Switching (ZVS). Now the new i_m is given as:

$$i_m(t) = i_m(t_3) - \frac{V_c}{L_m}(t - t_3) \quad (3)$$

With the negative current direction, the secondary side current is now expressed as:

$$i_s(t) = i_s(t_3)\cos w_r(t - t_3) - \frac{nV_c - V_{cr2}(t_3)}{Z_r}\sin w_r(t - t_3) \quad (4)$$

State 4: This is the last state in one cycle of conduction where all the switches are turned OFF for a small instant of time, similar to state 2 [12]. The current conduction path in state 4 is presented in Figure 7.

During this state, the capacitors C_{s2} and C_{s3} are charged by i_p and C_{s1} and C_{s4} are discharged. On the secondary side, the diode D2 is forward-biased, and the capacitors Cr1 and Co are discharged to the load.

The pulses for the HTFB converter are generated by the MPPT controller, which is discussed in the next section.

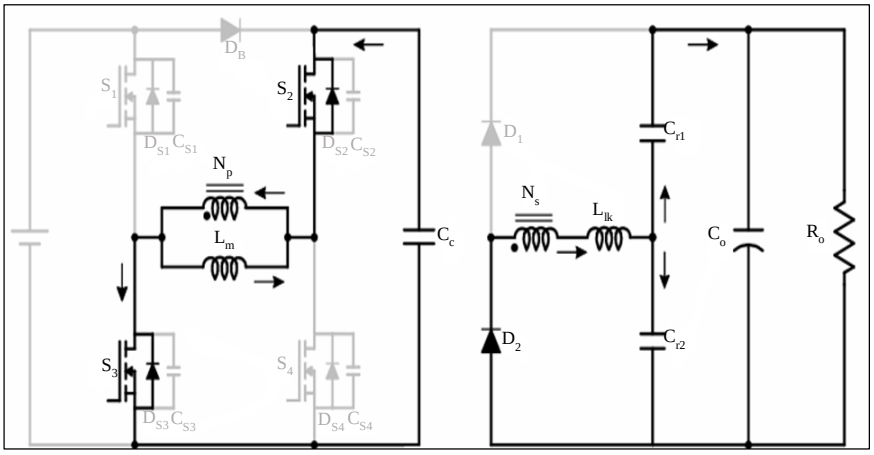

Fig. 6 State 3 operating condition

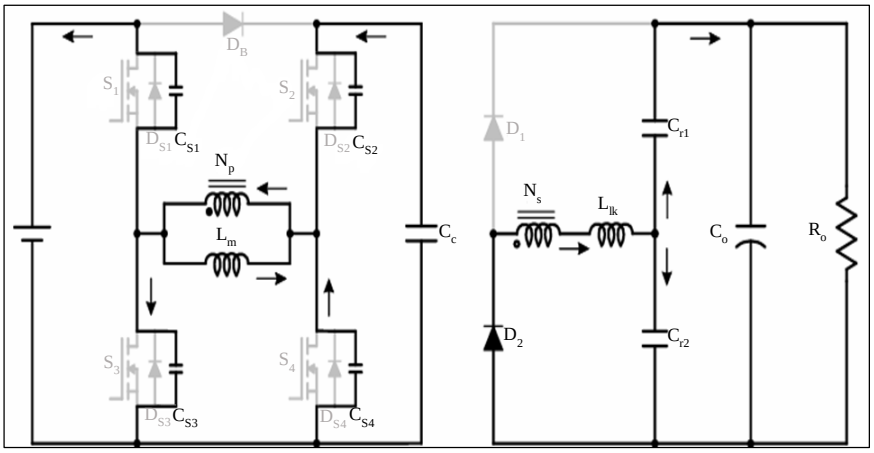

Fig. 7 State 4 operating condition

3. INC and FLC MPPTs Design

3.1. INC MPPT

Initially, the duty ratio for the switches is generated by INC MPPT, which takes voltage and current signal feedback from the PV array [13]. The conventional INC MPPT is the basic technique for maximum power extraction in many circuit systems. The schematic flow diagram of the INC MPPT can be observed in Figure 8.

The duty ratio is either increased or decreased as per the changes in the current and voltage ratio. The change in duty ratio is expressed as:

$$D_k = D_{k-1} + \Delta D \begin{cases} If\ dV \neq 0\ \&\ \frac{dI}{dV} > \frac{-I}{V} \\ If\ dV = 0\ \&\ dI > 0 \end{cases} \quad (5)$$

$$D_k = D_{k-1} - \Delta D \begin{cases} If\ dV \neq 0\ \&\ \frac{dI}{dV} < \frac{-I}{V} \\ If\ dV = 0\ \&\ dI < 0 \end{cases} \quad (6)$$

$$D_k = D_{k-1} \begin{cases} If\ dV \neq 0\ \&\ \frac{dI}{dV} = \frac{-I}{V} \\ If\ dV = 0\ \&\ dI = 0 \end{cases} \quad (7)$$

Here D_k is the present duty ratio, D_{k-1} is the previous duty ratio, dV and dI are changes in PV array voltage and

current respectively [14]. The ΔD is variable duty ratio value which increase or decreases the D_k. The INC MPPT is replaced with FLC MPPT for better stability and power extraction from the PV array.

3.2. FLC MPPT

For the FLC MPPT, the same signals from the PV are taken as input, and the required signals for the FLC are calculated. The FLC needs two input variables, I/V and dI/dV, generated by the present and past values of the voltage and current of the PV array [15]. The new FLC MPPT structure can be observed in Figure 9.

As per Figure 9, the input variables are segregated into multiple regions, R1 to R5, using five triangular Membership Functions (MFs) [16]. The output variable 'delD' also has five MFs. The input and output variables MFs are shown in Figure 10.

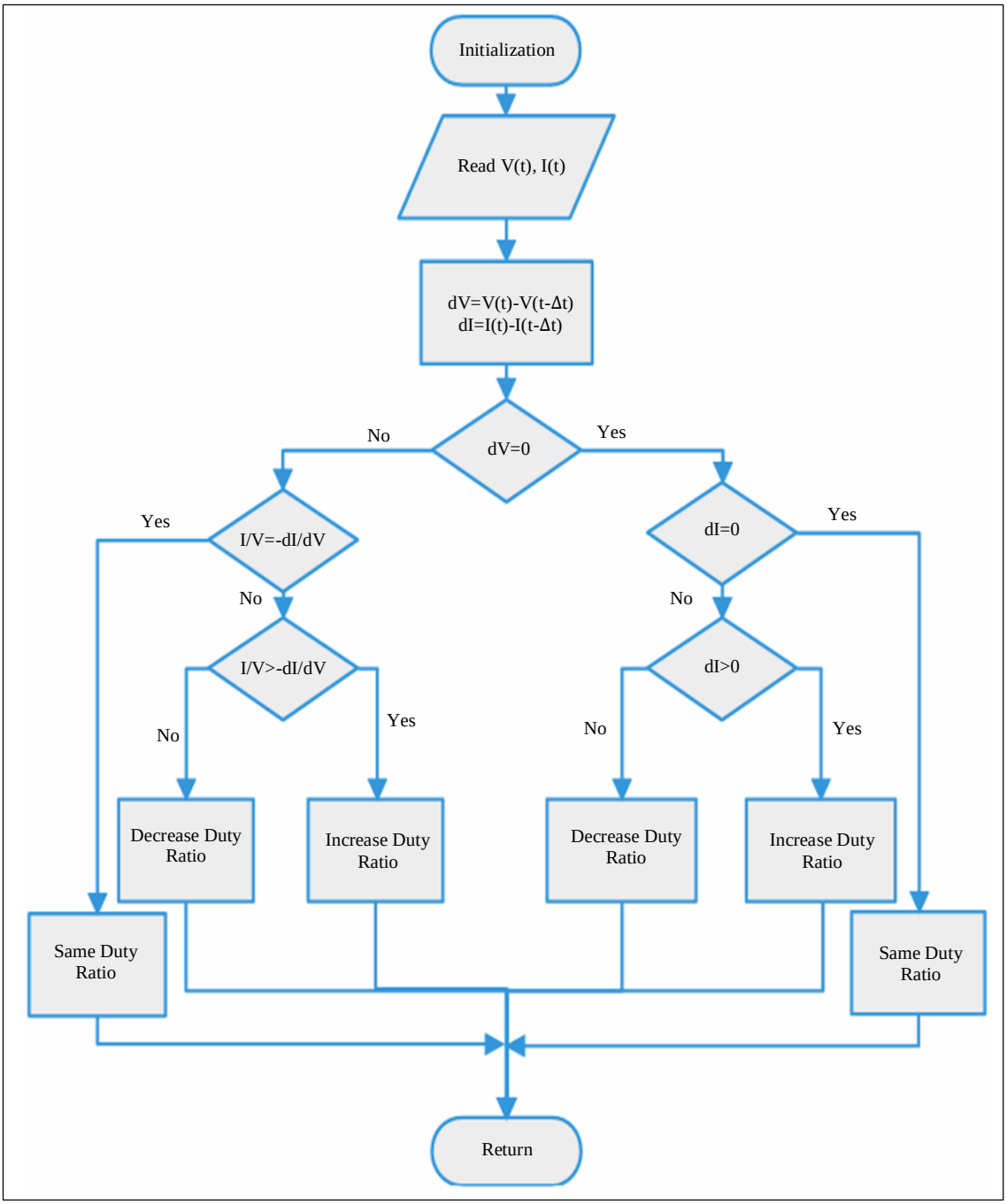

Fig. 8 INC MPPT schematic diagram

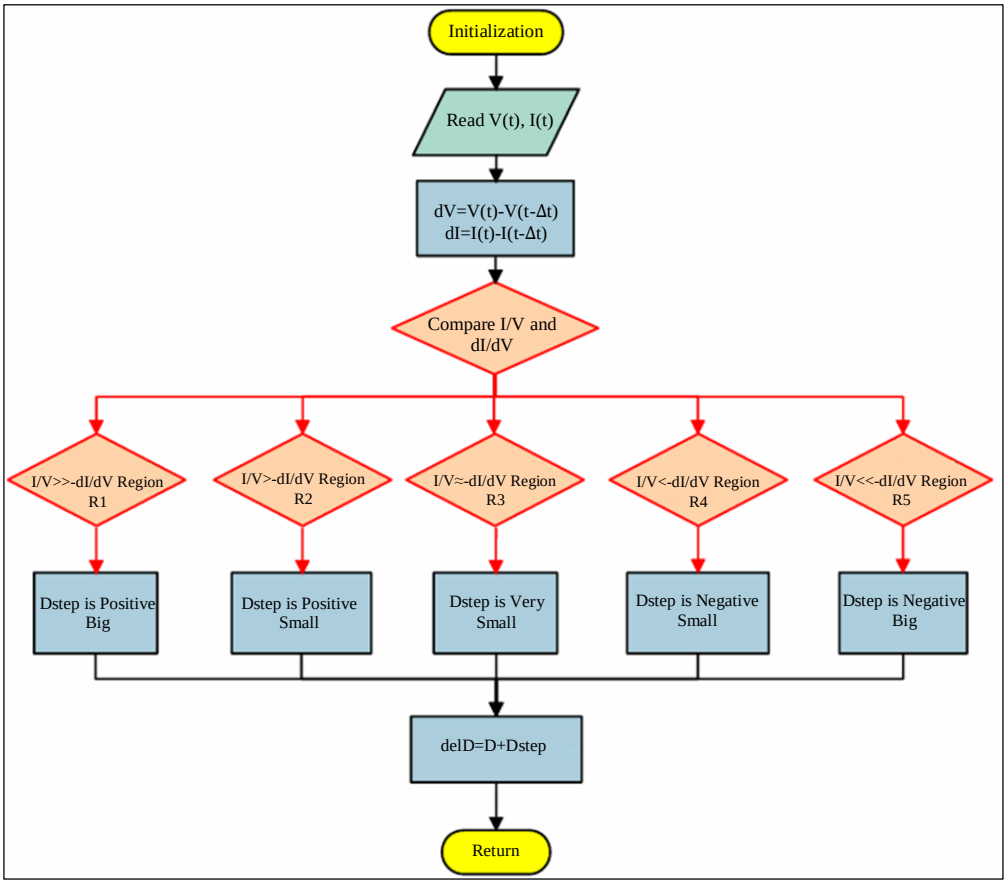

Fig. 9 FLC MPPT structure

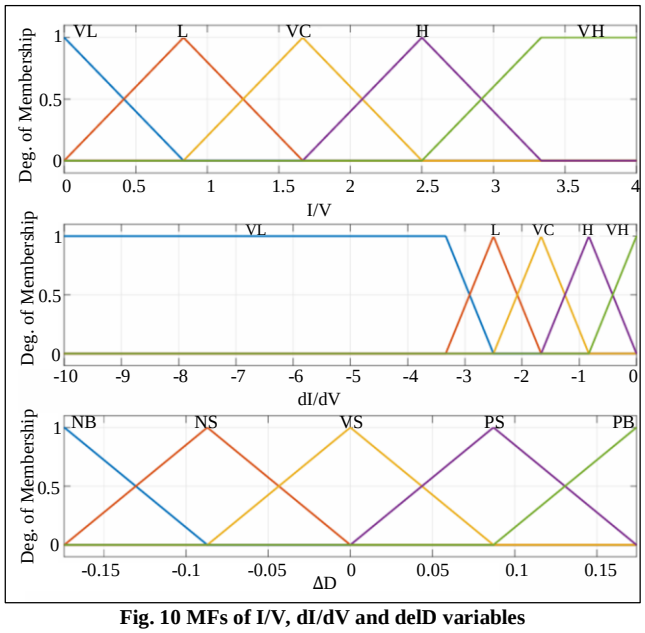

Fig. 10 MFs of I/V, dI/dV and delD variables

The names of the MFs are set as per the range given to the variables. The input variables MF names are given as VL (Very Large), L (Large), VC (Very Center), H (High) and VH (Very High). The output variable MF names are given as NB (Negative Big), NS (Negative Small), VS (Very Small), PS (Positive Small) and PB (Positive Big) [17]. These MFs are linked by rule Table 1 with 25 rule bases.

Table 1. 25 rule table

		dI/dV				
		VL	**L**	**VC**	**H**	**VH**
I/V	**VL**	PB	PS	PS	VS	NS
	L	PB	PS	VS	NS	NB
	VC	PB	PS	VS	NS	NB
	H	PB	PS	VS	NS	NB
	VH	PB	PS	PS	NS	NB

As per Table 1, the duty ratio of the switch is updated to the PWM generator, producing pulses for the switch S1-S4 of the HTFB.

4. Results and Discussion

The circuit structure with PV array, HTFB, VSC, EV charging circuit and utility grid is modelled, and both MPPTs are tested with different operating conditions. The below configuration Table 2 parameters are used for the simulation results using MATLAB Simulink software.

Table 2. System configuration parameters

Name of the Unit	Parameter values
PV array	V_{mp} = 29.42V, I_{mp} = 7.99A, V_{oc} = 36.96V, I_{sc} = 8.48A, N_p = 7, N_s = 6, P_{pv} = 9.8kW
HTFB	P_n = 10kVA, f_n = 50kHz, n = 2, L_m = 695µH
EV Charging Station	V_{nom_bat} = 250V, Capacity = 40Ah L_{buck} = 1mH, C_o = 1000µF, R_{igbt} = 0.01Ω V_{bat_ref} = 300V, I_{bat_ref} = 20A, K_{pv} = 0.1, K_{iv} = 0.023, K_{pc} = 0.0075, K_{ic} = 0.0002.
Inverter	R_{igbt} = 1mΩ, f_c = 5kHz, V_{dcref} = 500V, Lf = 250µH, Cf = 10kVAR
Utility Grid	2500MVA 132kV, 50Hz

The given parameters of each unit are updated in the simulation model and run with different operating conditions. The simulation time is set to 1sec and both the models with INC and FLC MPPT are simulated with a comparison of results in graphical representation.

Figure 11 has the characteristics of the PV array with constant solar irradiation of 1000W/mt^2 set from the initial simulation. The Vpv is recorded at 160V, which is boosted to 500V by the HTFB converter. The Ipv is 43A, resulting in 7kW of Ppv extraction for the given solar irradiation. Figure 12 is the boosted voltage measurement at the DC link or output terminals of HTFB.

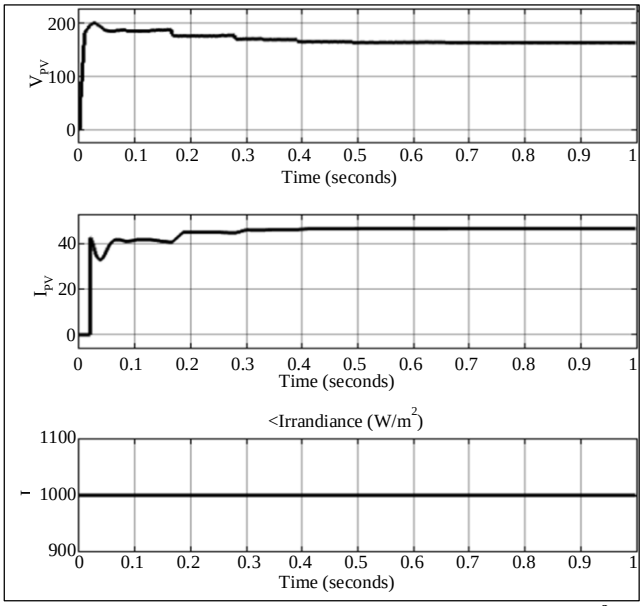

Fig. 11 PV characteristics with constant irradiation (1000W/mt^2)

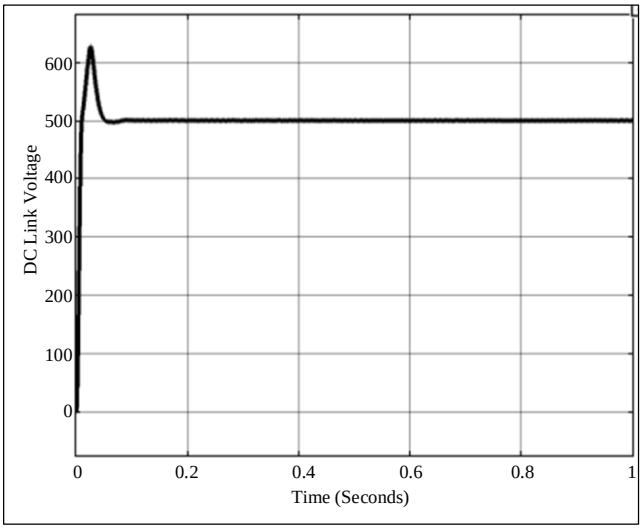

Fig. 12 DC link voltage or output voltage of HTFB converter

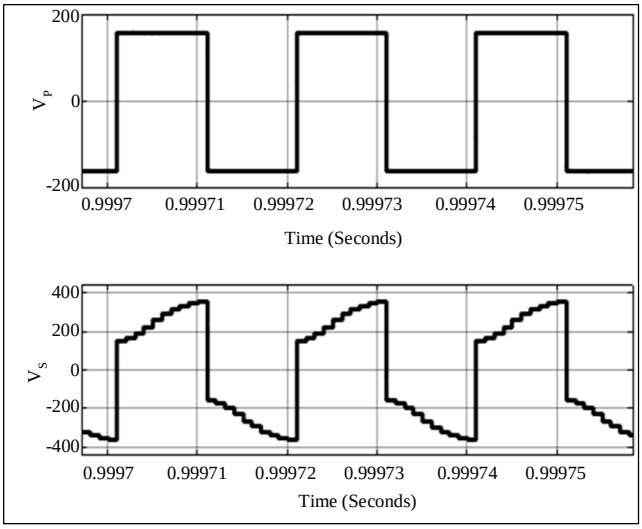

Fig. 13 HFTF primary and secondary winding voltages

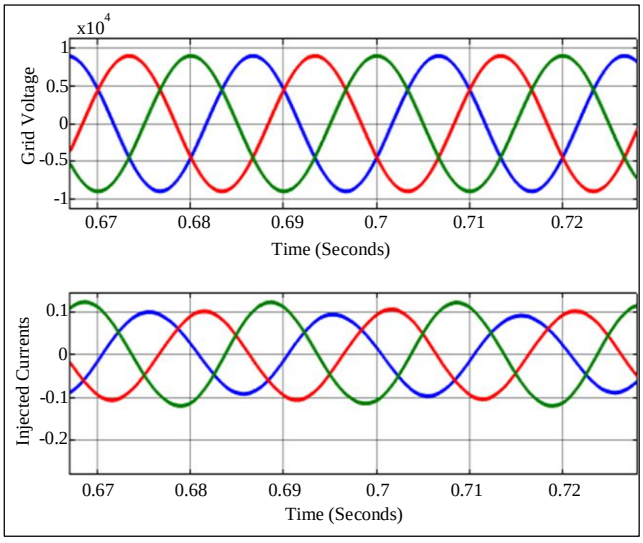

Fig. 14 Grid voltages and injected currents from renewable module inverter

For the given input of 160V DC from the PV array, the square AC voltage generation by the full bridge converter fed to the primary winding and induced boosted secondary winding voltage is presented in Figure 13. Figure 14 shows the three voltages and injected currents from the PV array HTFB inverter module. These are considered from the secondary side of the step-up transformer. Along with the grid shared current measurements, the EV battery characteristics of the charging station can be observed in Figure 15.

The rising EV SOC of the battery pack determines that the battery is charging. The negative 20A represents battery charging in MATLAB Simulink software. The voltage of the battery is 250V, which is the nominal voltage of the battery.

The INC MPPT is updated with FLC MPPT with a 25rule base, as presented in Figure 16. For the same solar irradiation, comparative results of different parameters are taken and are presented in Figure 17.

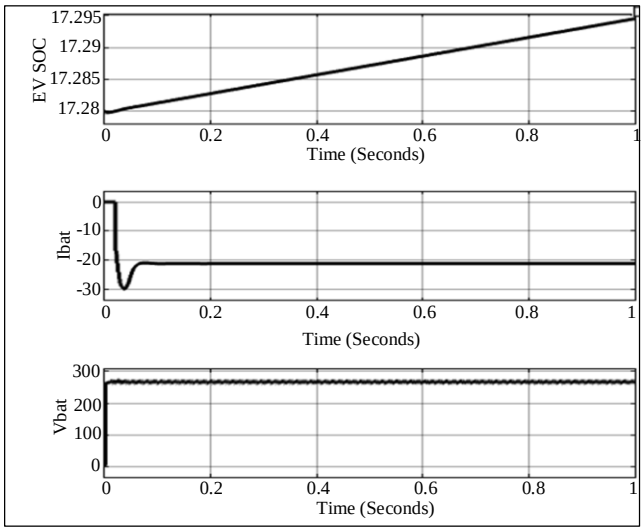

Fig. 15 EV battery characteristics

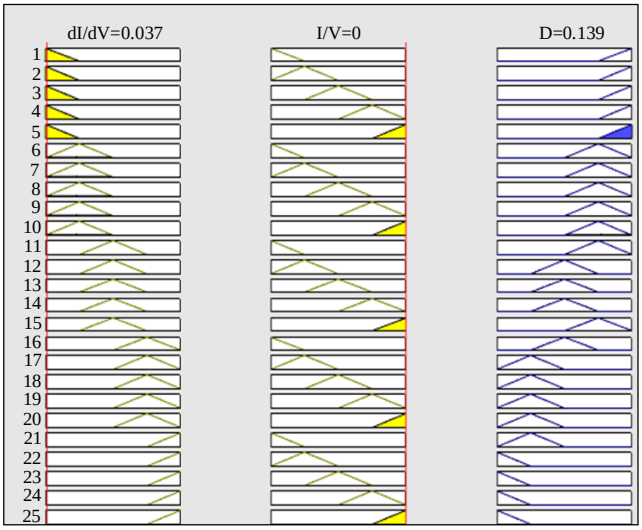

Fig. 16 FLC MPPT rule base

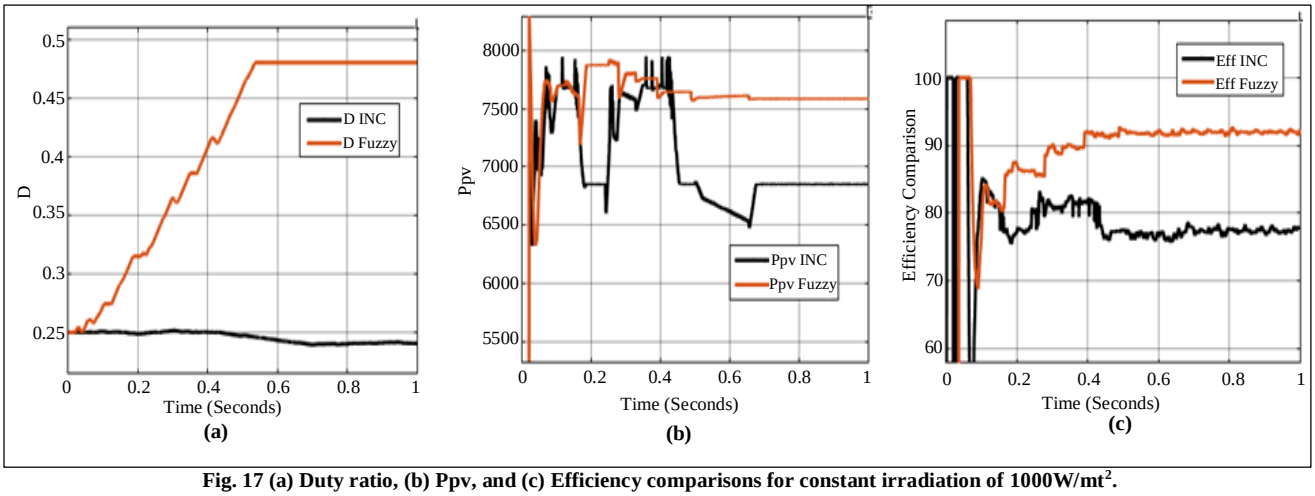

Fig. 17 (a) Duty ratio, (b) Ppv, and (c) Efficiency comparisons for constant irradiation of 1000W/mt^2.

Figure 17(a) is the duty ratio comparison, 17(b) is the extracted PV array comparison, and 17c is the efficiency comparison between INC and FLC MPPT topologies. As observed, the duty ratio generation of FLC MPPT is reaching the maximum point of 0.48 for the given solar irradiation. This results in extra power extraction at 7.6kW for FLC MPPT where it was 6.8kW for INC MPPT. An extra 800W has been extracted from the PV array by the FLC MPPT, resulting in increased efficiency of the HTFB from 78% to 92%, as presented in Figure 17c. The solar irradiation input to the PV array is varied at different instants of time in the 1-second simulation and the characteristics of the PV array are presented in Figure 18. As per the change in solar irradiation the current amplitude is varied with slight variation in the voltage.

For the variable irradiation input to the PV array, the HTFB converter efficiency comparison is presented in Figure 19. All the comparison graphs for the INC and FLC MPPT are compared with values in Table 3.

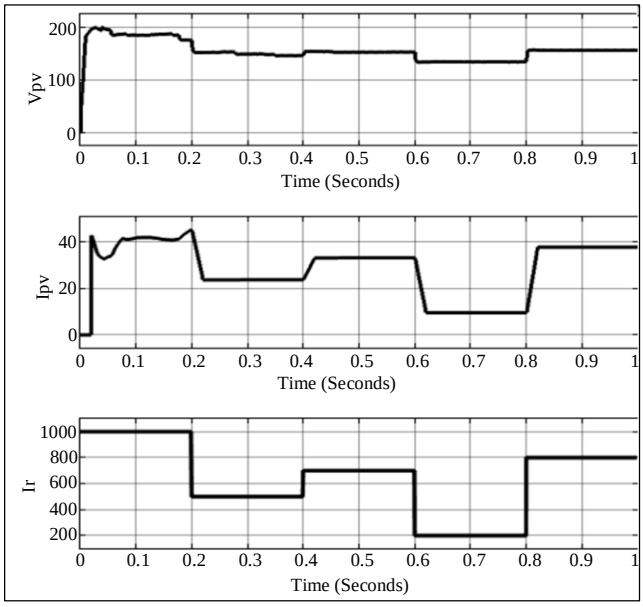

Fig. 18 PV characteristics with variable irradiation

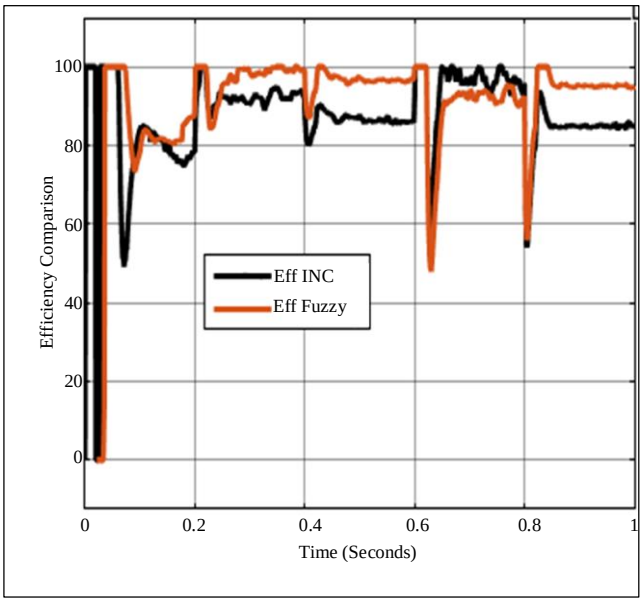

Fig. 19 Efficiency of the HTFB converter with variable solar irradiation

Table 3. INC vs FLC MPPT comparison table

Name of the Parameter	INC MPPT	FLC MPPT
Duty Ratio	0.25	0.48
Ppv	6.8kW	7.6kW
Efficiency	78%	92%

5. Conclusion

Successful modeling of the proposed system with a PV array connected to an HTFB DC/DC converter for efficient power extraction is achieved. The output of the HTFB is connected to a local EV charging station, charging the battery with the PV power through a buck converter circuit. At the same DC link point, a three-phase inverter is connected to share the excess PV power to the grid. As per the results generated in graphical format it is determined that the duty ratio estimation by the FLC is higher with FLC MPPT as compared to INC MPPT. This leads to extra power extraction of 800W from the PV array, increasing the efficiency to 92%, which was previously 78% for INC MPPT. This improves the performance of the complete system and stabilizes the voltages with a stable duty ratio generated by the FLC MPPT. Therefore, by the parameter comparison table 3, it is validated that the FLC MPPT for the HTFB converter generates better voltages and power for the system.

References

[1] M. Talaat et al., "Artificial Intelligence Applications for Microgrids Integration and Management of Hybrid Renewable Energy Sources," *Artificial Intelligence Review*, vol. 56, pp. 10557-10611, 2023. [CrossRef] [Google Scholar] [Publisher Link]

[2] Faisal R. Badal et al., "A Survey on Control Issues in Renewable Energy Integration and Microgrid," *Protection and Control of Modern Power Systems*, vol. 4, pp. 1-27, 2019. [CrossRef] [Google Scholar] [Publisher Link]

[3] David Rebollal et al., "Microgrid and Distributed Energy Resources Standards and Guidelines Review: Grid Connection and Operation Technical Requirements," *Energies*, vol. 14, no. 3, pp. 1-24, 2021. [CrossRef] [Google Scholar] [Publisher Link]

[4] Oladimeji Ibrahim et al., "Development of Observer State Output Feedback for Phase-Shifted Full Bridge DC-DC Converter Control," *IEEE Access*, vol. 5, pp. 18143-18154, 2017. [CrossRef] [Google Scholar] [Publisher Link]

[5] Shupeng Li et al., "A Hardware-Simplified Soft-Start Scheme for Current-Fed Full-Bridge DC-DC Converter," *Electronics*, vol. *13*, no. 1, pp. 1-14, 2024. [CrossRef] [Google Scholar] [Publisher Link]

[6] Avdhesh kumar, Rachana Garg, and Priya Mahajan, "Performance Analysis of Grid Integrated PV System Using SRF and IRPT Control," *2019 1st International Conference on Signal Processing, VLSI and Communication Engineering (ICSPVCE)*, Delhi, India, pp. 1-7, 2019. [CrossRef] [Google Scholar] [Publisher Link]

[7] Saban Ozdemir, Necmi Altin, and Ibrahim Sefa, "Fuzzy Logic Based MPPT Controller for High Conversion Ratio Quadratic Boost Converter," *International Journal of Hydrogen Energy*, vol. 42, no. 28, pp. 17748-17759, 2017. [CrossRef] [Google Scholar] [Publisher Link]

[8] Sung-Ho Lee et al., "Hybrid-Type Full-Bridge DC/DC Converter with High Efficiency," *IEEE Transactions on Power Electronics*, vol. 30, no. 8, pp. 4156-4164, 2015. [CrossRef] [Google Scholar] [Publisher Link]

[9] Qinglin Zhao et al., "A Hybrid Full-Bridge Converter with Wide Output Voltage for High-Power Applications," *IET Power Electronics*, vol. 13, no. 3, pp. 592-601, 2020. [CrossRef] [Google Scholar] [Publisher Link]

[10] Jaeil Baek, and Han-Shin Youn, "Full-Bridge Active-Clamp Forward-Flyback Converter with an Integrated Transformer for High-Performance and Low Cost Low-Voltage DC Converter of Vehicle Applications," *Energies*, vol. *13*, no. 4, pp. 1-17, 2020. [CrossRef] [Google Scholar] [Publisher Link]

[11] Devaraj Elangovan et al., "Design, Simulation and Implementation of Current Fed Isolated Full Bridge DC-DC with Voltage Multiplier for Fuel Cell Grid Applications," *Energy Procedia*, vol. 90, pp. 574-586, 2016. [CrossRef] [Google Scholar] [Publisher Link]

[12] Jiye Liu et al., "Comparison of Boost and LLC Converter and Active Clamp Isolated Full-Bridge Boost Converter for Photovoltaic DC System," *The Journal of Engineering*, vol. 2019, no. 16, pp. 3007-3011, 2019. [CrossRef] [Google Scholar] [Publisher Link]

[13] Derek Ajesam Asoh, Brice Damien Noumsi, and Edwin Nyuysever Mbinkar, "Maximum Power Point Tracking Using the Incremental Conductance Algorithm for PV Systems Operating in Rapidly Changing Environmental Conditions," *Smart Grid and Renewable Energy*, vol. 13, no. 5, pp. 89-108, 2022. [CrossRef] [Google Scholar] [Publisher Link]

[14] Abdelkhalek Chellakhi et al., "An Enhanced Incremental Conductance MPPT Approach for PV Power Optimization: A Simulation and Experimental Study," *Arabian Journal for Science and Engineering*, 2024. [CrossRef] [Google Scholar] [Publisher Link]

[15] Mahmoud N. Ali et al., "An Efficient Fuzzy-Logic Based Variable-Step Incremental Conductance MPPT Method for Grid-Connected PV Systems," *IEEE Access*, vol. 9, pp. 26420-26430, 2021. [CrossRef] [Google Scholar] [Publisher Link]

[16] R.K. Rai, and O.P. Rahi, "Fuzzy Logic Based Control Technique Using MPPT for Solar PV System," *2022 First International Conference on Electrical, Electronics, Information and Communication Technologies (ICEEICT)*, Trichy, India, pp. 1-5, 2022. [CrossRef] [Google Scholar] [Publisher Link]

[17] Lalit Kumar Narwat, and Javed Dhillon, "Design and Operation of Fuzzy Logic Based MPPT Controller under Uncertain Condition," *Journal of Physics: Conference Series*, vol. 1854, pp. 1-12, 2020. [CrossRef] [Google Scholar] [Publisher Link]